Supplementary Information

A Dual-Facet Mechanism in Copper Nanocubes for Electrochemical CO_2 Reduction into Ethylene

Giulia Mangione,[†§] Jianfeng Huang,[‡] Raffaella Buonsanti,[‡] Clémence Corminboeuf[*†]

†Laboratory for Computational Molecular Design (LCMD), Institute of Chemical Sciences and Engineering, Ecole Polytechnique Fédérale de Lausanne, CH-1015 Lausanne, Switzerland

‡ Laboratory of Nanochemistry for Energy (LNCE), Department of Chemical Sciences and Engineering, Ecole Polytechnique Fédérale de Lausanne, CH-1950 Sion, Switzerland

[§]National Center for Computational Design and Discovery of Novel Materials (MARVEL), Ecole Polytechnique Fédérale de Lausanne (EPFL), 1015 Lausanne, Switzerland

*E-mail: clemence.corminboeuf@epfl.ch.

1. Experimental Section: Structural Analysis of the CuNCs

The synthesis and the electrocatalytic studies of the CuNCs are reported in our previous works.[1,2] Here, additional structural analysis was performed using TEM (see Figure 1). The low resolution TEM image was acquired on a FEI Tecnai-Spirit (at 120 kV). The HR-TEM image was acquired on a FEI Titan Themis 60–300 operated at 300 kV.

2. Computational Method

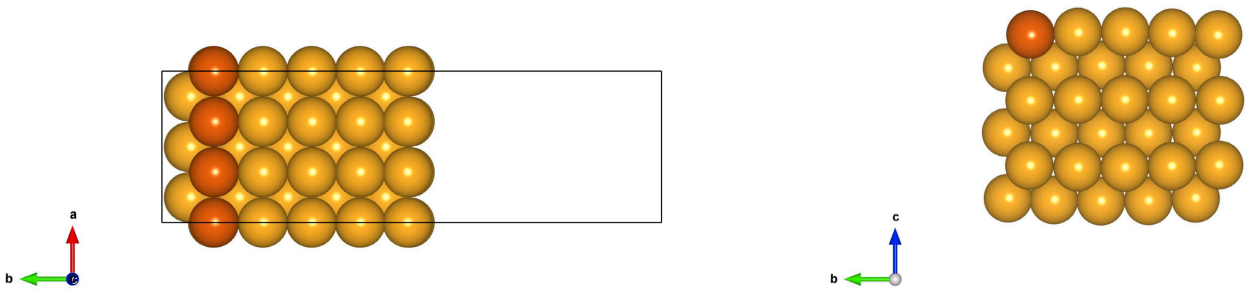

Figure S1. (a) Top and (b) side views of the 1D nanowire model of CuNC. The orange spheres represent the {110}-like edge and the yellow ones represent the terraces.

The computations were carried out using the software Quantum ESPRESSO.[3] For all atoms, the interaction between core and valence electrons were described using the GBRV Ultrasoft pseudopotentials[4] with the inclusion of scalar relativistic effects on the copper at the generalized gradient approximation Perdew, Burke and Ernzerhof (PBE) level.[5,6] Long-range dispersion interactions were accounted for using Grimme's -D2 semi-empirical dispersion correction.[7] The Kohn-Sham equations were solved using kinetic energy cutoffs of 100 Ry and 800 Ry for the wave functions and charge densities, respectively. The optimization of the bulk lattice constants of the face-centered cubic copper and the estimation of the adsorption energies over the CuNC model in **Figure S1** were carried out by sampling the Brillouin zone with a Monkhorst-Pack grid with a *k*-point density of 0.2 points per $Å^{-1}$.[8] The calculated lattice constant of copper was 3.63 Å, in agreement with the experimental value (3.62 Å).[9] The CuNCs were modelled as a 1D nanowire

periodic in *a* direction from a six-layer slab cleaved in the {100} direction with vacuum along *b* axis. This resulted in two edge terminations in *y* direction, namely {100}- and {110}-like edges, where the latter was chosen for representing the{100} terrace/{110} edge interface (see **Figure** S1). To separate the slabs from their periodic images vacuum values of 15 Å and 23 Å were chosen along *b* and *c* axes, respectively. Finally, the wire width of 5 Cu atoms in the *y* direction was used to ensure that the active sites on the {110}-like edge were not affected by those in the {100} direction. The adsorption energies of the various intermediates bound to the CuNC surface were computed keeping the three bottom layers fixed at the bulk positions and allowing the full relaxation of the three topmost ones and of the adsorbates. A dipole correction along the *c* direction was applied in all the cases. The adsorption energies were evaluated minimizing the atomic forces below 0.05 eV·Å^{-1}. The reaction energies at each step of the CO_2 electrochemical reduction were computed as DFT energy differences between the surface-bound products and reactants involved in it. The gas phase DFT energies of CO_2, H_2O and $\frac{1}{2}\,H_{2\,(g)}$, according to the Computational Hydrogen Electrode (CHE) model,[10–12] were used as reference. The CHE model is based on equilibrium between the proton-electron couple ($H^{+}_{(aq)} + e^{-}$) and H_2 at 1 atm and 0 V *vs.* the standard hydrogen electrode. At any pH value, the following reaction is used as the reference potential:

$$H^{+}_{(aq)} + e^{-} \rightarrow \frac{1}{2}\,H_{2\,(g)} \tag{S.1}$$

The chemical potential of $\frac{1}{2}\,H_{2\,(g)}$ is equivalent to that of the couple ($H^{+}_{(aq)} + e^{-}$) in aqueous solution. As such, the DFT energy of $\frac{1}{2}\,H_{2\,(g)}$ rather than that of the proton-electron couple was used as the electrochemical reference.[10–12]

Finally, the activation energies of the non-electrochemical steps of the *CO dimerization and *CO-*COH coupling were calculated using the climbing image nudged elastic band.[13] To locate the transition states, the minimum energy paths were examined using 11-15 images, including the initial and final states. Owing to the large and asymmetric supercells associated with our systems, the computed energies (see equations (1) and (4) in the main text) do not include ZPE and free-energy corrections and follow references 14 and 15.

3. Adsorption energies of intermediates

The adsorption energies of the various intermediates formed on CuNC surface during the electrochemical CO_2 reduction (CO_2RR) proceeding through paths A and B are given in **Tables S1-S6.**

Table S1. Adsorption energies (in eV) of the intermediates formed through the reaction pathway A at the {100} terrace/{110} edge interface of the CuNC surface.

Intermediate	Adsorption energy
2 *CO_2	-0.44
2 *COOH	-0.31
2 *CO	-0.32
Dimer $A_{\{100\}}$	1.10
Dimer $B_{\{100\}}$	1.11
*COCOH (from Dimer $A_{\{100\}}$)	0.06
*COCOH (from Dimer $B_{\{100\}}$)	-0.27
*CCO (from Dimer $A_{\{100\}}$)	-1.50
*CCO (from Dimer $B_{\{100\}}$)	-1.19

Table S2. Adsorption energies (in eV) of the intermediates formed through the reaction pathway A at the {110} terrace/{110} edge interface of the CuNC surface.

Intermediate	Adsorption energy
2 *CO_2	-0.62
2 *COOH	-0.39
2 *CO	-0.16
Dimer $A_{\{110\}}$	1.24
Dimer $B_{\{110\}}$	1.25
*COCOH (from Dimer $A_{\{110\}}$)	-0.21
*COCOH (from Dimer $B_{\{110\}}$)	-0.15
*CCO (from Dimer $A_{\{110\}}$)	-0.94
*CCO (from Dimer $B_{\{110\}}$)	-1.01

Table S3. Adsorption energies (in eV) of the intermediates formed through the reaction pathway A on the pure Cu(100) terrace.

Intermediate	Adsorption energy
2 *CO_2	-0.44
2 *COOH	-0.10
2 *CO	-0.42
*COCO	1.12
*COCOH	-0.06
*CCO	-1.48

Table S4. Adsorption energies (in eV) of the intermediates formed through the reaction pathway B at the {100} terrace/{110} edge interface of the CuNC surface.

Intermediate	Adsorption energy
2 *CO_2	-0.44
2 *COOH	-0.31
2 *CO	-0.32
*CO *COH	0.58, 0.87
*COCOH	0.14, -0.10
*CCO	-1.07, -1.11

Table S5. Adsorption energies (in eV) of the intermediates formed through the reaction pathway B at the {110} terrace/{110} edge interface of the CuNC surface.

Intermediate	Adsorption energy
2 *CO_2	-0.62
2 *COOH	-0.39
2 *CO	-0.16
*CO *COH	0.90, 1.25
*COCOH	-0.01, -0.35
*CCO	-0.78, -0.80

Table S6. Adsorption energies (in eV) of the intermediates formed through the reaction pathway B on the pure Cu(100) terrace.

Intermediate	Adsorption energy
2 *CO_2	-0.44
2 *COOH	-0.10
2 *CO	-0.42
*CO *COH	0.43

*COCOH	0.21
*CCO	-1.06

4. Transition state structures

Figure S2 reports the structures of the transition states as well as of the initial and final states for the non-electrochemical C-C coupling step through *CO dimerization and *COH-*CO coupling. Only the transition states of the coupling process with the lowest activation energies are reported. **Figure S4** gives the energy profiles of the two competing mechanisms on the two facets ({100} terrace / {110} edge and {110} terrace / {110} edge in comparison with that of the pure (100) terrace.

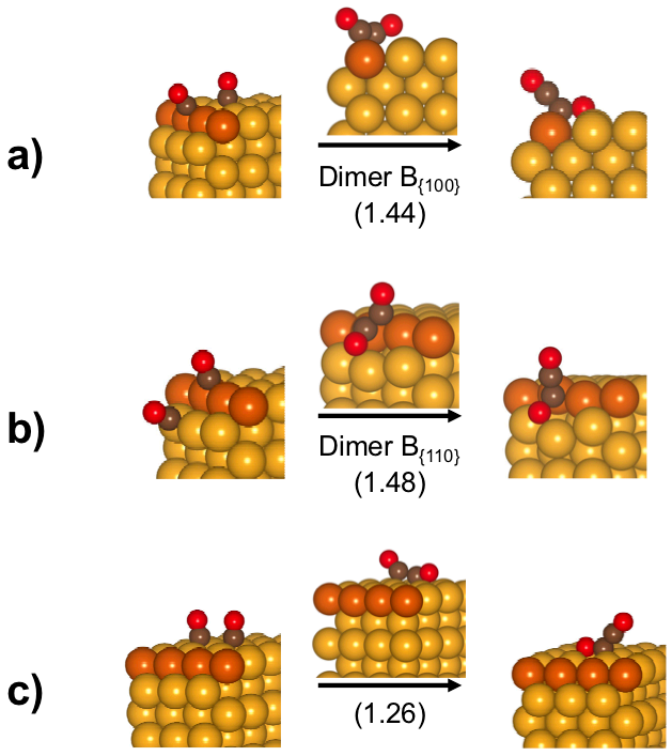

Figure S2. Structure of the initial (left), transition (middle) and final (right) states of the non-electrochemical C-C coupling step through *CO dimerization on the a) {100} terrace / {110} edge,

b) {110} terrace / {110} edge interfaces and c) on the pure Cu(100) terrace. The values in parentheses represent the activation energies of the coupling (in eV).

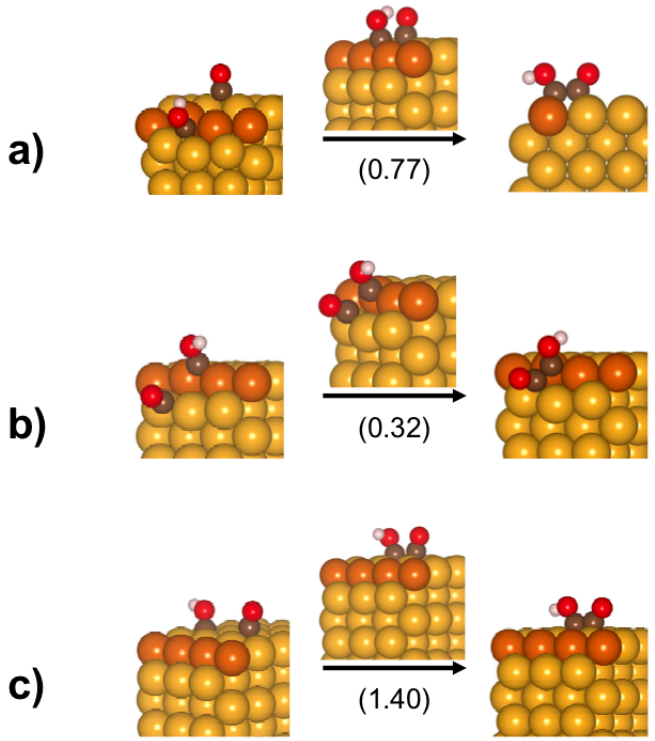

Figure S3. Structure of the initial (left), transition (middle) and final (right) states of the non-electrochemical C-C coupling step through *COH-*CO coupling on the a) {100} terrace / {110} edge, b) {110} terrace / {110} edge interfaces and c) on the pure Cu(100). The values in parentheses represent the activation energies of the coupling (in eV).

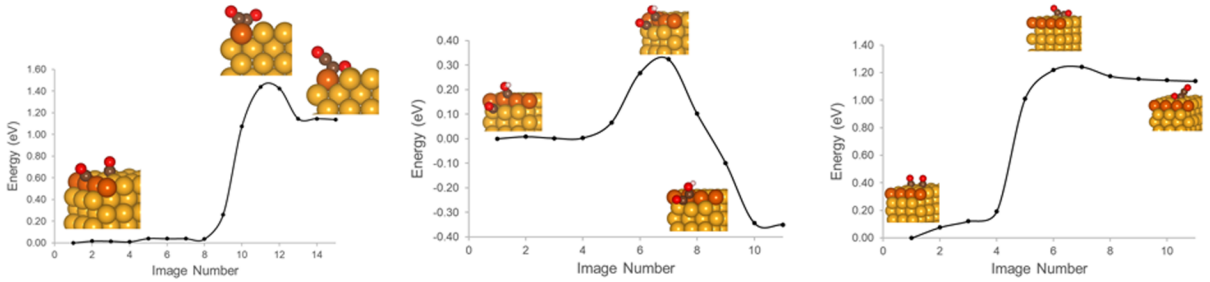

Figure S4. Energy profiles of the two competing coupling mechanisms on the two facets {100} terrace / {110} edge (left) and {110} terrace / {110} edge (middle) having the lowest C-C formation barriers. The energy profile of *CO dimerization taking place on the pure (100) terrace is reported for comparison (right).

REFERENCES

(1) Loiudice, A.; Lobaccaro, P.; Kamali, E. A.; Thao, T.; Huang, B. H.; Ager, J. W.; Buonsanti, R. Tailoring Copper Nanocrystals towards C_2 Products in Electrochemical CO_2 Reduction. *Angew. Chem. Int. Ed.,* **2016**, *55*, 5789–5792.

(2) Huang, J.; Hörmann, N.; Oveisi, E.; Loiudice, A.; De Gregorio, G. L.; Andreussi, O.; Marzari, N.; Buonsanti, R. Potential-Induced Nanoclustering of Metallic Catalysts during Electrochemical CO_2 Reduction. *Nat. Commun.* **2018**, *9*, 3117–3125.

(3) Giannozzi, P.; Baroni, S.; Bonini, N.; Calandra, M.; Car, R.; Cavazzoni, C.; Ceresoli, D.; Chiarotti, G. L.; Cococcioni, M.; Dabo, I.; et al. QUANTUM ESPRESSO: A Modular and Open-Source Software Project for Quantum Simulations of Materials. *J. Phys.: Condens. Matter* **2009**, *21*, 395502–395518.

(4) Garrity, K. F.; Bennett, J. W.; Rabe, K. M.; Vanderbilt, D. Pseudopotentials for High-Throughput DFT Calculations. *Comput. Materi. Sci.* **2014**, *81*, 446–452.

(5) Perdew, J. P.; Burke, K.; Ernzerhof, M. Generalized Gradient Approximation Made Simple. *Phys. Rev. Lett.* **1996**, *77*, 3865–3868.

(6) Perdew, J. P.; Burke, K.; Ernzerhof, M. Generalized Gradient Approximation Made Simple. *Phys. Rev. Lett.* **1997**, *78*, 1396–1396.

(7) Grimme, S. Semiempirical GGA-Type Density Functional Constructed with a Long-Range Dispersion Correction. *J. Comput. Chem.* **2006**, *27*, 1787–1799.

(8) Monkhorst, H. J.; Pack, J. D. Special Points for Brillouin-Zone Integrations. *Phys. Rev. B* **1976**, *13*, 5188–5192.

(9) Straumanis, M. E.; Yu, L. S. Lattice Parameters, Densities, Expansion Coefficients and Perfection of Structure of Cu and of Cu–In α Phase. *Acta Crystallogr. A* **1969**, *25*, 676–682.

(10) J. K. Nørskov; J. Rossmeisl; A. Logadottir; Lindqvist, L.; Kitchin, J. R.; Bligaard, T.; Jónsson, H. Origin of the Overpotential for Oxygen Reduction at a Fuel-Cell Cathode. *J. Phys. Chem. B* **2004**, *108*, 17886–17892.

(11) Rossmeisl, J.; Logadottir, A.; Nørskov, J. K. Electrolysis of Water on (Oxidized) Metal Surfaces. *Chem. Phys.* **2005**, *319*, 178–184.

(12) Rossmeisl, J.; Qu, Z. W.; Zhu, H.; Kroes, G. J.; Nørskov, J. K. Electrolysis of Water on Oxide Surfaces. *J. Electroanal. Chem.* **2007**, *607*, 83–89.

(13) Henkelman, G.; Jónsson, H. Improved Tangent Estimate in the Nudged Elastic Band Method for Finding Minimum Energy Paths and Saddle Points. *J. Chem. Phys.* **2000**, *113*, 9978–9985.

(14) Huang, Y.; Handoko, A. D.; Hirunsit, P.; Yeo, B. S. Electrochemical Reduction of CO_2 Using Copper Single-Crystal Surfaces: Effects of CO* Coverage on the Selective Formation of Ethylene. *ACS Catal.* **2017**, *7*, 1749–1756.

(15) Montoya, J. H.; Peterson, A. A.; Nørskov, J. K. Insights into C-C Coupling in CO_2 Electroreduction on Copper Electrodes. *ChemCatChem* **2013**, *5*, 737–742.